Int. J. Electrochem. Sci., 9 **(2014)** 6821 - 6833

International Journal of
ELECTROCHEMICAL
SCIENCE
www.electrochemsci.org

Scan Rate Dependent Morphology of Polyaniline Films Electrochemically Deposited on Nickel

Andrea Kellenberger[1,*], *Daniela Ambros*[1], *Nicoleta Plesu*[2]

[1] University Politehnica Timisoara, Faculty of Industrial Chemistry and Environmental Engineering, 300006 P-ta Victoriei 2, Timisoara, Romania
[2] Romanian Academy, Institute of Chemistry, Bd. Mihai Viteazul 24, 300223 Timisoara, Romania
[*]E-mail: andrea.kellenberger@upt.ro

Received: 3 July 2014 / *Accepted:* 4 September 2014 / *Published:* 29 September 2014

The effect of scan rate on the morphology and properties of polyaniline has been investigated for samples deposited electrochemically on nickel from sulfuric acid solution. A nanofibrilar network structure has been obtained for low scan rates (10, 25 and 50 mV s^{-1}) whereas for the highest scan rate (100 mV s^{-1}) the structure was more compact, the nanofibrils aggregated and their features were not very obvious. Both diameter and length of nanofibers are scan rate dependent, decreasing from 140 to 90 nm and from 1.35 to 0.72 μm when the scan rate is increased from 10 to 50 mV s^{-1}. The nanofiber network tends to be more compact and with less free-volume as the scan rate is increased. Generally, high specific capacitances and low charge transfer resistance values are obtained for all nanofibrilar polyaniline films as compared to the compact structure. The optimum scan rate for deposition was found to be 25 mV s^{-1}, leading to the highest specific capacitance and lowest charge transfer resistance.

Keywords: Polyaniline nanofibers, scan rate, nickel, electrochemical impedance spectroscopy

1. INTRODUCTION

Polyaniline is an intrinsic conducting polymer that has been intensively investigated due to its versatile use in a large number of practical applications, i.e. the fabrication of electrochemical storage devices, sensors, biosensors, anticorrosive coatings. Polyaniline can be obtained by either chemical or electrochemical oxidative polymerization. Chemical polymerization has the advantage of producing large scale quantities of polymer, but electrochemical polymerization allows a more rigorous control of synthesis parameters and is useful when polymer film electrodes are needed. The synthesis method and processing conditions play an important role in tailoring polymer properties, i.e. morphology and as a

consequence conductivity, which is one of the main properties of conducting polymers, particularly of polyaniline [1,2].

Different morphologies have been reported for polyaniline obtained by chemical oxidative synthesis depending on the molar ratio of oxidant to monomer [3]. Also, by changing the molar ratio of acid to monomer, nanoflakes, nanorods or nanospheres have been obtained in selenious acid [4] and respectively nanotubes, nanoflakes and nanofiber networks in dichloroacetic acid [5]. Polyaniline nanofibers with diameters of 20-50 nm have been reported in the presence of soft templates such as polyethylene glycol [6]. It has been shown that acidity changes in the initial stages of polymerization also have an influence on polyaniline morphology obtained by interfacial polymerization, allowing a controlled synthesis of PANI micro/nanostructures [7]. Besides acidity, another factor that affects the size of polyaniline nanofibers obtained by interfacial polymerization is the polarity of the organic solvent [8].

The morphology obtained by means of electrochemical synthesis is less varied than with chemical oxidation methods due to the ease of controlling synthesis parameters. The main factors affecting morphology in electrochemical synthesis are the nature of the doping anion [9], the electrode material [10,11], pH [12], scan rate in potentiodynamic deposition [13,14] and deposition time in potentiostatic deposition [15]. It has been found that varying the potential scan rate of only the first cycle from 100 to 2 mV s^{-1} induces changes from globular to fibrilar-like morphology [16], explained by different nucleation mechanisms. Frequently reported morphologies for electrochemical deposited polyaniline are nanofibers or nanofiber networks, as a consequence of the growth mechanism described as a two stages mechanism [10,17]. In the first stage, after the nucleation sites are deposited on the electrode surface, they tend to grow predominantly in the horizontal direction and form a compact 2D polyaniline layer. In the second stage, the polymerization takes place preferentially in the vertical direction and polyaniline nanofibers grow on the previously deposited compact layer and not directly on the bare electrode surface.

In this paper we report on the effect of potential scan rate on the morphology and properties of polyaniline films electrochemically deposited on nickel electrode. It is shown that the morphology changes from a compact structure at higher scan rates to porous nanofibrilar morphology at lower scan rates. There is also a clear correlation between morphological changes and electrochemical impedance spectra. The charge transfer resistance and specific capacitance of polyaniline films are controlled by their structure and morphology.

2. EXPERIMENTAL

Aniline (puriss., p.a., ≥ 99.5% GC from Fluka) was freshly distilled under reduced pressure and stored in dark at low temperature. Distilled water and analytical grade sulfuric acid (95-97% from Merck) were used to prepare the electrolyte solutions. Before measurements the Ni electrode was mechanically polished with SiC paper of different grades from 400 to 2400 and then mirror polished with diamond sprays with different grain size (6 and 3 μm). The freshly prepared electrode was immediately immersed in the electrolyte solution and cyclic voltammograms were taken.

The electrochemical polymerization of aniline was carried out by cyclic voltammetry using an Autolab PGSTAT 302N. All measurements were performed in a conventional one-compartment, three-electrode electrochemical cell equipped with a nickel disc working electrode (A = 0.64 cm^2), two graphite rods as counter electrode and silver/silver chloride (Ag/AgCl) as reference electrode. Cyclic voltammograms were recorded at different scan rates of 10, 25, 50 and 100 mV s^{-1} from 0.1 mol L^{-1} aniline in 0.5 mol L^{-1} H_2SO_4 solutions. The potential was scanned from –0.15 V to 1.25 V for the first cycles to allow the initiation of the polymerization process, afterwards the reversal potential was decreased to 0.85 V to avoid the overoxidation reactions of the polymer chain. The cyclic voltammograms were interrupted after reaching a current of about 0.01 A for the first oxidation peak, corresponding to a current density of about 0.016 A cm^{-2}. The prepared samples are denoted as Pani 10, Pani 25, Pani 50 and respectively Pani 100, indicating the scan rate applied in the potentiodynamic scan during the deposition of the polymer films. Electrochemical properties of polyaniline films were investigated by cyclic voltammetry and electrochemical impedance spectroscopy (EIS) in monomer free H_2SO_4 solution. EIS measurements were carried out in the frequency range from 0.1 Hz to 100 kHz and AC voltage amplitude of 10 mV. For each spectrum 60 points were collected, with a logarithmic distribution of 10 points per decade. The experimental electrochemical impedance data were fitted to the electrical equivalent circuit by a complex non-linear least squares Levenberg–Marquardt procedure using ZView 3.0 software (Scribner Associates, Inc.).

The morphology and structure of the polyaniline films prepared on nickel were characterized by field emission scanning electron microscopy (FE-SEM) using a QUANTA FEG 250 scanning electron microscope. Fourier-transformed infrared (FTIR) spectra of prepared polyaniline were measured on KBr pellets using a Shimadzu IR PRESTIGE 21 spectrometer. For each spectrum 20 interferograms with a resolution of 4 cm^{-1} were sampled.

3. RESULTS AND DISCUSSION

Fig. 1a and b show examples of cyclic voltammograms recorded during the two stage deposition of Pani films on nickel electrode.

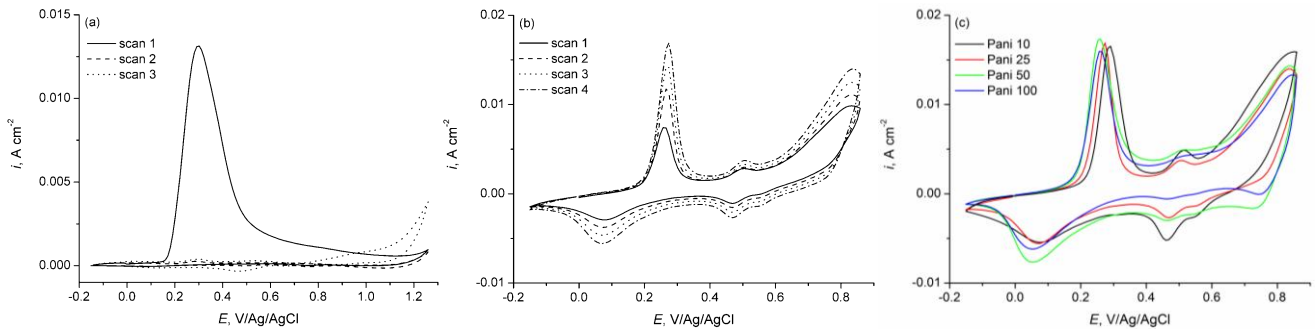

Figure 1. Potentiodynamic deposition of Pani from 0.1 mol L^{-1} aniline in 0.5 mol L^{-1} H_2SO_4 solution on nickel electrode, scan rate 25 mV s^{-1}: initiation step (a) and growth step (b). Last scan corresponding to the growth of the four Pani films (c).

In the first stage (Fig. 1a), CVs were recorded in a large potential window corresponding to the induction or initiation of the polymerization reaction. In the next stage (Fig. 1b), during the growth of the polymer film, the upper potential limit was shifted to lower values to avoid the oxidative degradation reactions and consecutive CVs were taken in a narrower potential window.

An irreversible oxidation peak appears in the first anodic scan (Fig. 1a), that has been assigned to the oxidation of the nickel electrode. In the following cycles, the oxidation peak is absent which shows that the electrode is in a passive state and allows the electrooxidation of aniline at an electrode potential of about 1V. Typical CVs have been recorded during the growth of Pani films, characterized by the presence of two pairs of redox peaks corresponding to redox transitions from leucoemeraldine to emeraldine and from emeraldine to pernigraniline. Also, an intermediate pair of redox peaks is assigned to secondary degradation reactions. The potential peak of the first redox transition shifts slightly to lower potentials as the scan rate increases. The corresponding anodic / cathodic peak potentials are 0.290 / 0.077 V at 10 mV s^{-1}; 0.275 / 0.070 V at 25 mV s^{-1}; 0.258 / 0.055 V at 50 mV s^{-1}; and respectively 0.258 / 0.052 V at 100 mV s^{-1}. It can be also noticed that the intensity of the degradation peaks is more pronounced at lower scan rates. An important feature related to the growth of conducting polymer films is the continuous increase of the current and charge corresponding to the first anodic peak during consecutive potential cycling. The dependence of charge associated to the first peak versus the number of scans is given in Fig. 2.

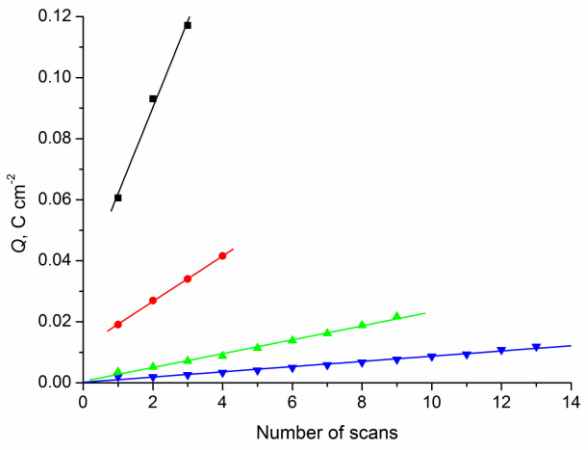

Figure 2. Dependence of charge on the number of scans for: Pani 10 (■), Pani 25 (●), Pani 50 (▲) and Pani 100 (▼).

In all cases a linear dependence is observed which indicates a continuous growth of the polymer film proportional to the number of potential scans. However, the charge corresponding to the first anodic peak is quite different, indicating that films with different thicknesses have been obtained. The highest growth rate of the polyaniline film is obtained for the lowest scan rate, as indicated by the steepest slope.

The mass of deposited polyaniline was estimated according to Faraday's law of electrolysis, assuming a current efficiency of 100%. Also, the thickness of Pani films was calculated for an average density of polyaniline of 1.4 g cm^{-3}.

$$m = \frac{(M_m + 0.5M_a)Q}{(2+0.5)F} \quad (1)$$

where: m is the mass of deposited Pani, g, M_m and M_a are the molar masses of aniline monomer (93.13 g mol^{-1}) and hydrogen sulfate (97 g mol^{-1}), Q is the total deposition charge and F is the Faraday constant (F = 96485 C mol^{-1}).

The capacitance of polymer films can be determined by either cyclic voltammetry or electrochemical impedance spectroscopy. In cyclic voltammetry the polymer film capacitance is obtained from the slope of the linear dependence of capacitive current density versus scan rate. The capacitive current density is calculated as the average of anodic and cathodic currents obtained from the cyclic voltammograms given in Fig. 3.

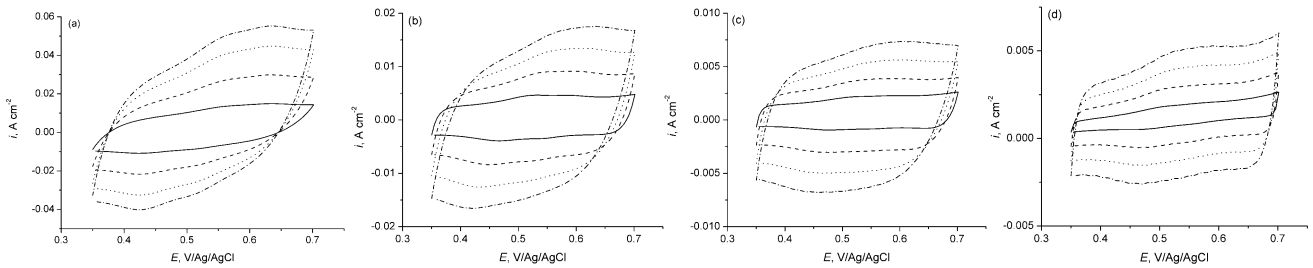

Figure 3. Cyclic voltammograms of Pani 10 (a), Pani 25 (b), Pani 50 (c) and Pani 100 (d) in 0.5 mol L^{-1} H_2SO_4 solution at 50 mV s^{-1} (——), 100 mV s^{-1} (- - - -), 150 mV s^{-1} (·····) and 200 mV s^{-1} (-·-·-·-).

The dependence of the capacitive current density on scan rate is illustrated in Fig. 4 for all four polyaniline samples.

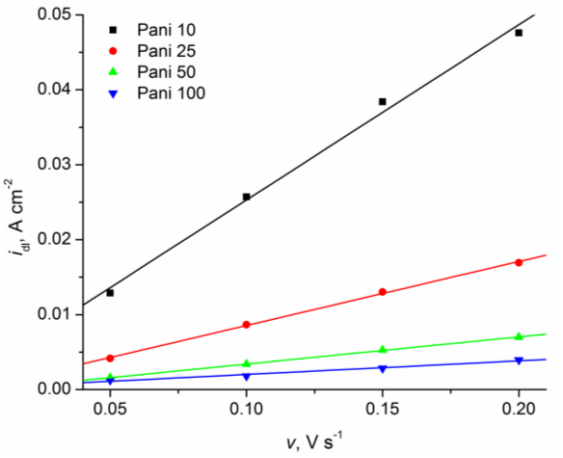

Figure 4. Dependence of the capacitive current density on scan rate.

Film thickness and capacitance values determined from both cyclic voltammetry and impedance data are given in Table 1. Also, specific capacitance values were calculated according to:

$$C_S = \frac{C_{CV}}{m} \tag{2}$$

where: C_{CV} is capacitance determined from cyclic voltammetry and m is the mass of deposited Pani determined with equation (1).

It can be observed that, as expected, the capacitance of Pani films increases proportionally to film thickness and mass of deposited Pani. However, when specific capacitance values are compared, the highest capacitance is obtained for Pani 25, and the lowest capacitance is obtained for Pani 100 due to different morphology, as it will be discussed based on FE-SEM imaging.

Table 1. Thickness and capacitance values of Pani samples.

Sample	d [μm]	C_{CV} [F cm^{-2}]	C_{EIS} [F cm^{-2}]	C_S [F g^{-1}]
Pani 10	2.55	0.233	0.255	655
Pani 25	0.85	0.085	0.095	715
Pani 50	0.44	0.036	0.041	585
Pani 100	0.22	0.018	0.023	490

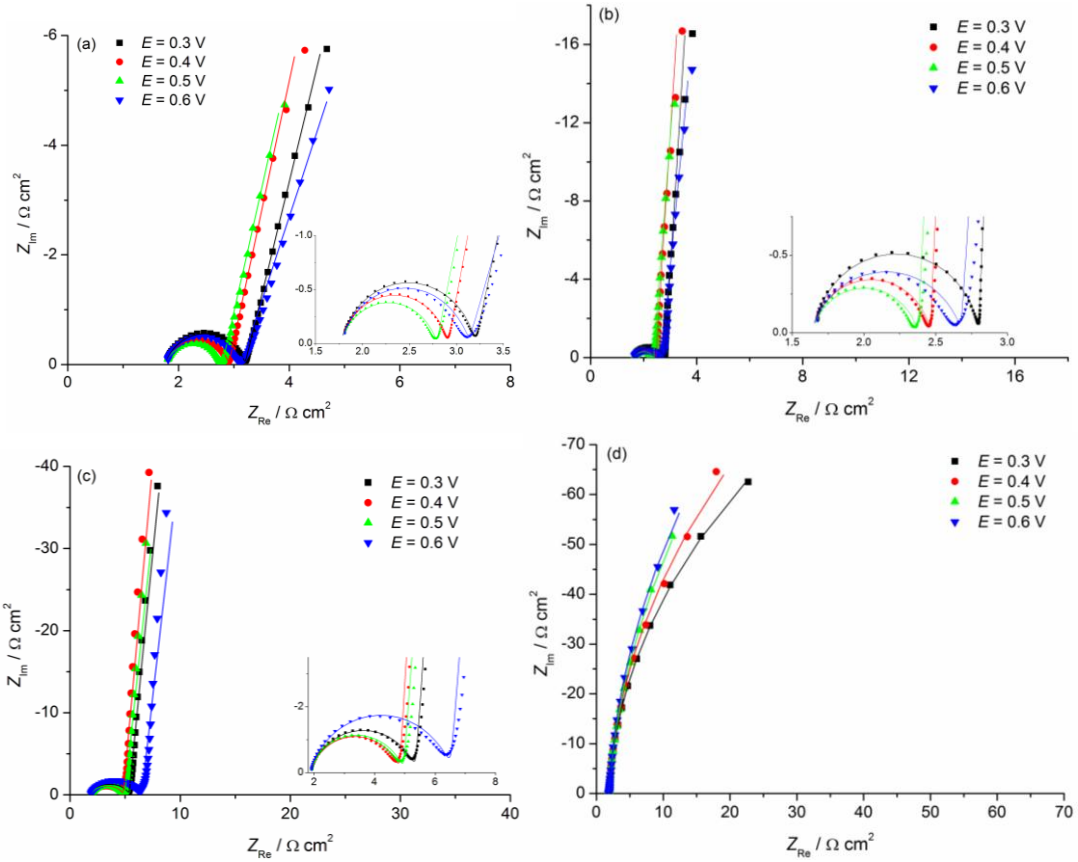

Figure 5. Series of Nyquist plots of Pani 10 (a), Pani 25 (b), Pani 50 (c) and Pani 100 (d) measured in 0.5 mol L^{-1} H_2SO_4 solution at different potentials. Symbols are experimental data and the continuous line represents the results of modeling to the equivalent electric circuit.

The influence of polyaniline morphology and applied potential on the impedance response was investigated. Electrochemical impedance spectra were collected at several electrode potentials, placed in the region were the polyaniline films are in the conductive form. Typical examples of EIS spectra taken for the polyaniline films at electrode potentials above 0.2 V are given in Fig. 5.

The impedance behavior in the potential window from 0.2 to 0.6 V is assumed to be a characteristic of Pani/electrolyte interface and of Pani layer pseudocapacitance [18,19]. The changes in impedance parameters were used to interpret processes taking place inside polyaniline and at the polyaniline/electrolyte interface as a consequence of morphology changes. The shape of the complex plane plots depends on both polymer film thickness and morphology. For Pani 10, Pani 25 and Pani 50, with similar morphologies, the complex plane plots are characterized by the appearance of a high frequency semicircle followed by a near vertical line at low frequencies, at all investigated electrode potentials. The impedance response at high frequencies corresponds to the charge transfer at the polyaniline/electrolyte interface and low frequency response is dominated by the polyaniline film capacitance. As the film thickness decreases, the imaginary part of the impedance increases, indicating a decrease of the low frequency capacitance. The diameter of the high frequency semicircle is potential dependent decreasing up to potential of 0.4 – 0.5 V, in agreement with the transition from leucoemeraldine to the conductive emeraldine form of Pani. A completely different behavior is observed for Pani 100, where an incomplete arc of a semicircle with larger diameter can be seen.

The equivalent electric circuit used to analyze EIS data is presented in Fig. 6 and contains a series connection of the charge transfer resistance R_{ct} and the polymer film capacitance expressed by a constant phase element CPE-2, in parallel with the double layer capacitance expressed by CPE-1. In case of Pani 100 the impedance data were fitted assuming only a constant phase element in parallel with a resistance.

Table 2. Values of the circuit elements obtained by fitting the impedance data to the equivalent circuit.

Sample	E [V]	R_S [Ω]	CPE-T_1 [F cm^{-2} s^{n-1}]	n_1	R_{ct} [Ω cm^2]	CPE-T_2 [F cm^{-2} s^{n-1}]	n_2	χ^2
Pani 10	0.3	1.8	1.41×10^{-4}	0.85	1.44	0.255	0.85	1.9×10^{-4}
	0.4	1.8	1.52×10^{-4}	0.85	1.14	0.261	0.87	3.1×10^{-4}
	0.5	1.8	2.49×10^{-4}	0.81	1.03	0.318	0.86	5.6×10^{-4}
	0.6	1.8	$^{*}2.14 \times 10^{-4}$	0.82	1.37	0.288	0.80	1.2×10^{-3}
Pani 25	0.3	1.7	6.79×10^{-5}	0.92	1.15	0.095	0.97	1.7×10^{-4}
	0.4	1.6	1.06×10^{-4}	0.89	0.82	0.095	0.97	2.8×10^{-4}
	0.5	1.6	$*2.01 \times 10^{-4}$	0.84	0.74	0.123	0.96	6.7×10^{-4}
	0.6	1.6	$*2.54 \times 10^{-4}$	0.82	1.05	0.110	0.96	1.7×10^{-3}
Pani 50	0.3	1.9	2.41×10^{-4}	0.80	3.50	0.042	0.95	4.6×10^{-4}
	0.4	1.9	2.29×10^{-4}	0.81	2.97	0.041	0.95	6.9×10^{-4}
	0.5	1.9	2.48×10^{-4}	0.80	3.11	0.052	0.94	8.6×10^{-4}
	0.6	1.9	2.27×10^{-4}	0.82	4.67	0.047	0.94	8.2×10^{-4}
Pani 100	0.3	1.9	0.023	0.98	237	-	-	2.7×10^{-4}
	0.4	1.9	0.230	0.97	301	-	-	2.5×10^{-4}
	0.5	1.9	0.030	0.97	387	-	-	2.8×10^{-4}
	0.6	1.9	0.027	0.98	392	-	-	5.5×10^{-4}

* Relative standard errors above 10%.

The results of fitting together with the goodness of fit, expressed by the Chi-squared value are given in Table 2. There is a good agreement between experimental results and fitted data, as indicated by small relative standard errors, generally bellow 10%, and low Chi-squared values.

The constant phase element in the equivalent circuit replaces the capacitance, since it describes more accurately the behaviour of real systems. The impedance of a constant phase element is given by:

$$Z_{CPE} = T^{-1} (j\omega)^{-n} \quad (3)$$

where T is a parameter related to the double layer capacity, n is an exponent between 0 and 1 and ω is the angular frequency.

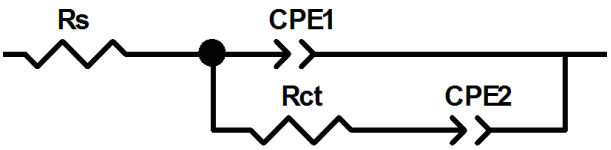

Figure 6. Equivalent electric circuit used to fit the impedance data.

The charge transfer resistance of Pani 10, Pani 25 and Pani 50 decreases up to an electrode potential of 0.4 – 0.5 V, where polyaniline is in its conductive form, emeraldine, and increases again at more positive potentials, according to Fig. 7a. The lowest values of charge transfer resistance are obtained for Pani 25 and Pani 10, with a highly porous, nanofibrilar morphology, whereas for Pani 100 R_{ct} values are two orders of magnitude higher, corresponding to a much lower conductivity, explained by its compact morphology. The specific capacitance of Pani films, calculated as the ratio between capacitance determined by EIS and mass, is given in Fig. 7b as a function of electrode potential. It shows the presence of a maxima at 0.5 V corresponding to the potential of the lowest resistance. Highest capacitances are obtained for Pani 25 and Pani 10, in agreement with voltammetric data.

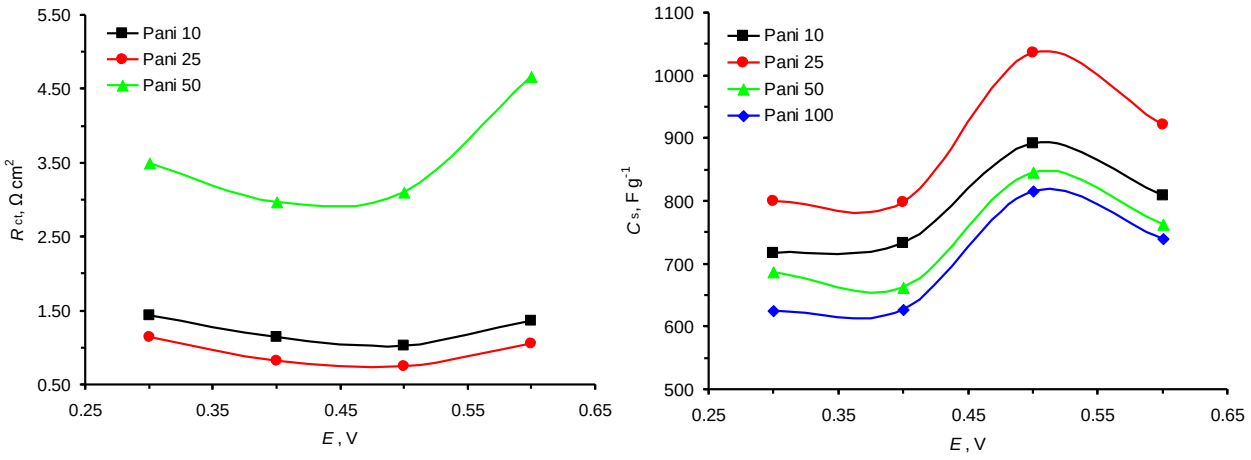

Figure 7. Charge transfer resistance and specific capacitance as a function of potential.

The lower resistance and higher capacitance of Pani films obtained at low scan rates are a result of different morphology. It has been shown that conductivity and apparent charge carrier mobility are enhanced for nanofibrilar Pani as compared to granular Pani having the same oxidation levels [20]. In

fibrilar morphology the chains are extended, more ordered and allow the existence of delocalized states along the chain length direction. In granular morphology the chains are coiled up which tends to localize the electronic states [21], thus explaining the higher conductivity of polyaniline nanofibers.

A similar increase in conductivity appears during oxidation of Pani, explained by the conformational changes that take place, consisting in the stretching of the polymer chains from a compact coil structure to an extended or relaxed coil [1]. It has been reported that the formation of polaron lattice induces both a stretching of polymer chains and an increase in charge carrier mobility [22]. Polymer chains expand due to the increase of the electrostatic repulsion forces between polarons located on the polymer backbone. As the distance between the positive charges on the chain increases, the PANI chains become more linear and the coiled structure relaxes [23].

Fig. 8 gives the FE-SEM images of Pani films on nickel for different scan rates used in the potentiodynamic deposition.

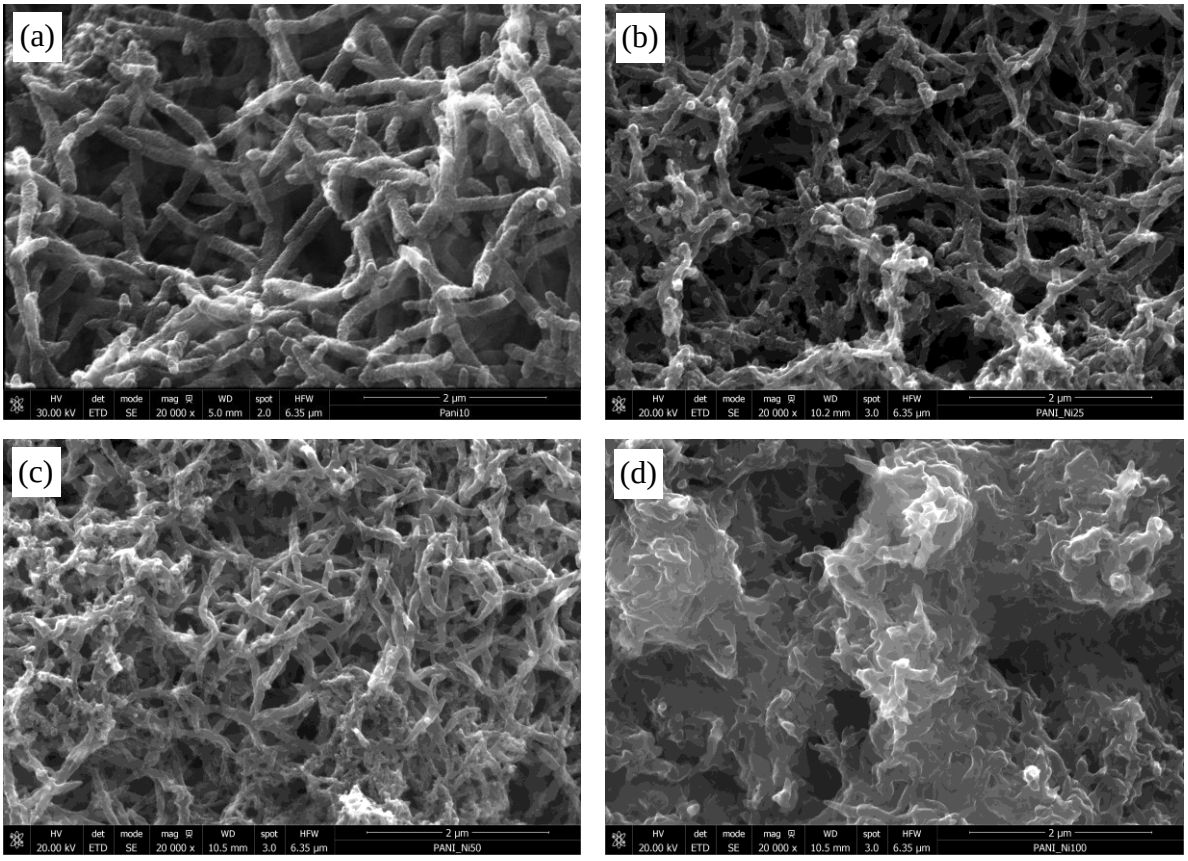

Figure 8. FE-SEM images of polyaniline films: Pani 10 (a), Pani 25 (b), Pani 50 (c) and Pani 100 (d).

Polyaniline samples obtained at scan rates of 10, 25 and 50 mV s^{-1} show a porous, open, highly branched nanofibrilar structure, whereas samples obtained at 100 mV s^{-1} are composed of very short nanofibrils, almost completely merged with each other, resulting in a compact, stratified structure. For Pani 10 there is a high amount of long and smooth nanofibers while for Pani 50 some inclusions of

granular polyaniline could be observed. The nanofiber network tends to be more compact and with less free-volume as the scan rate is increased. The average diameter and length of the nanofibers decrease with the potentiodynamic scan rate applied for deposition in the following order: Pani 10 (140 nm / 1.35 μm) > Pani 25 (100 nm / 1.06 μm) > Pani 50 (90 nm / 0.72 μm). These results are consistent with literature data [13] and can be explained based on the mechanism of nucleation and growth of the polymer film. At low scan rates the number of nucleation sites generated at the surface of the nickel electrode is small, but their dimensions are bigger since the electrode is maintained for a longer time at the oxidation potential value. At higher scan rates the number of nucleation sites is higher, but their size is reduced. As a result a larger number of nanofibers with smaller diameters will be obtained. Also, some of the nanofibers present nodules on their surface, which can act as nucleation sites for future fibers leading to a highly branched structure.

The nanofibers' aspect ratio (L/D) varies in the order: Pani 25 (10.6) > Pani 10 (9.6) > Pani 50 (8.0) which might explain the highest capacitance and lowest resistance of Pani 25. It has been reported that high conductivities are obtained for branched Pani nanofibers with high aspect ratio, where charge carriers are free to move throughout the length of nanofibers and further extend to the branch regions, leading to an increased delocalization of charge [24]. The ability to transport charge carriers along the polymer backbone due to an extended conjugation length represents the intrachain conductivity, whereas the ability of carriers to hop between polymer chains represents the interchain conductivity.

Structural characterization of polyaniline films has been performed by FTIR spectroscopy and characteristic spectra for all samples are given in Fig. 9.

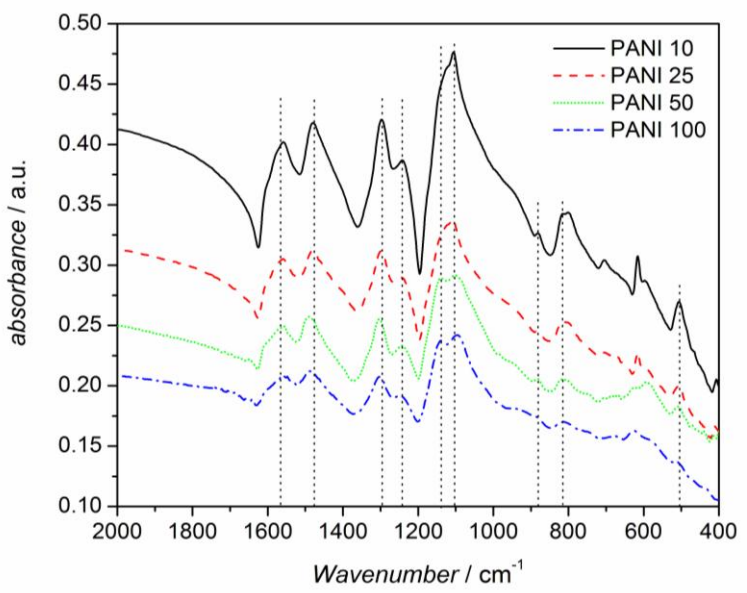

Figure 9. FTIR spectra of electrochemically synthesized polyaniline films.

The main vibrations observed in the FTIR spectra correspond to the C=C stretching vibration of the quinoid (1556 cm^{-1}) and benzenoid rings (1480 cm^{-1}). Also, the C–N stretching of the secondary

aromatic amine is observed at 1296 cm^{-1}. The band at 1240 cm^{-1} is characteristic for the conducting protonated form of PANI, it has been assigned to $C-N^{\bullet+}$ stretching in the polaron lattice [25] and it is present in the Raman spectra around 1250 cm^{-1} [26]. The very intense band at 1140 cm^{-1} has been ascribed to the vibration of the charged polymer units $Q=NH^{+}–B$ or $B–NH^{+}–B$ formed during doping [27] and it is considered to be a measure of electron delocalization in PANI, indicating its high conductivity. A contribution to the band at 1140 cm^{-1} may also originate from the aromatic in-plane C–H deformation vibration and from SO_3 asymmetric stretching vibration in the hydrogen sulfate counterion [28]. The aromatic C–H out-of-plane deformation observed at 816 cm^{-1} is consistent with the 1,4-substitution of the benzene ring.

FTIR studies carried out on polyaniline nanostructures have generally revealed a similar backbone structure to that of granular polyaniline. The main differences associated with the formation of Pani nanotubes / nanofibers are usually related to the presence of phenazine units and hydrogen bonds between neighboring chains [11,29-33]. Indication about the presence of phenazine units have been found by the presence of characteristic vibrations at 1623, 1415, 1450, 1208, 1144, 1136 and 1108 cm^{-1} [30-35] but some of these vibrations are difficult to assign because they overlap with characteristic vibrations of Pani. A vibration at 880 cm^{-1} indicates branching in the polymer chain and it is attributed to a 2- or 2,3-substituted phenazine ring [35-38].

The FTIR spectra of Pani films obtained at different scan rates contain few evidence about the presence of phenazine units, residing mainly in the presence of a vibration at 881 cm^{-1} for Pani 10, Pani 25 and Pani 100, which is absent in the spectra of Pani 100, and respectively the vibration at 705 cm^{-1} corresponding to the ring out-of plane deformation of monosubstituted phenylene ring. However, the assignment of the bands associated with the formation of Pani nanotubes is rather difficult and still open to discussion [33].

4. CONCLUSIONS

Polyaniline nanofibers have been synthesized by a potentiodynamic method on nickel. The morphology of the polyaniline films is affected by the scan rate, the average diameter and length of the nanofibers decreases with the scan rate. At scan rates of 10, 25 and 50 mV s^{-1} the nanofibers are interwoven in a porous network structure which tends to be more compact and with less free-volume as the scan rate increases. At 100 mV s^{-1} the nanofibrils becomes very short, they coalesce and form a much more compact structure. The morphology changes induce different properties of polyaniline films. Thus, films deposited at lower scan rates show high values of surface related capacitances, due to the increase of both thickness and electrochemically active surface area. However, comparing mass related capacitances, the best results are obtained for Pani 25. The optimum scan rate applied for deposition of Pani in this work, leading to best performances in terms of specific capacitance and charge transfer resistance, was found to be 25 mV s^{-1} and it is supposed to originate from an optimum combination of intrachain and interchain transport of charge carries.

ACKNOWLEDGEMENT
This work was supported by the Sectoral Operational Programme Human Resources Development, financed from the European Social Fund and by the Romania Government under the contract number POSDRU/86/ 1.2./S/58146 (MASTERMAT). We thank Prof. C. Pacurariu and M. Vagyon from the Faculty of Industrial Chemistry and Environmental Engineering for help with the FTIR measurements.

References

1. A.G. MacDiarmid, A.J. Epstein, *Synth. Met.*, 65 (1994) 103-116.
2. S.K. Jeong, J.S. Suh, Oh EJ, Y.W. Park, Kim CY, A.G. MacDiarmid, *Synth. Met.*, 69 (1995) 171-172.
3. C. Zhou, J. Han, R. Guo, *Macromolecules*, 41 (2008) 6473-6479.
4. C.A. Amarnath, J. Kim, K. Kim, J. Choi, D. Sohn, *Polymer*, 49 (2008) 432-437.
5. H. Wang, Y. Lu, *Synth. Met.*, 162 (2012) 1369-1374.
6. W. Zhao, L. Ma, K. Lu, *J. Polym. Res.*, 14 (2007) 1-4.
7. Y. Li, Y. Wang, X. Jing, R. Zhu, *J. Polym. Res.*, 18 (2011) 2119-2131.
8. P. Singh, R.A. Singh, *Synth. Met.*, 162 (2012) 2193-2200.
9. Y. Guo, Y. Zhou, *Eur. Polym. J.*, 43 (2007) 2292-2297.
10. N.T. Kemp, J.W. Cochrane, R. Newbury, *Synth. Met.*, 159 (2009) 435-444.
11. A. Kellenberger, N. Plesu, M. Tara-Lunga Mihali, N. Vaszilcsin, *Polymer*, 54 (2013) 3166-3174.
12. X.-Y. Peng, F. Luan, X.-X. Liu, D. Diamond, K.-T. Lau, *Electrochim. Acta*, 54 (2009) 6172-6177.
13. S. Mu, Y. Yang, *J. Phys. Chem. B*, 112 (2008) 11558-11563.
14. A. Cot, S. Lakard, J. Dejeu, P. Rougeot, C. Magnenet, B. Lakard, M. Gauthier, *Synth. Met.*, 162 (2012) 2370-2378.
15. N. Li, YH. Xiao, CZ. Xu, HH. Li, XD. Yang, *Int. J. Electrochem. Sci.*, 8 (2013) 1181-1188.
16. G.T. Andrade, M.J. Aguirre, S.R. Biaggio, *Electrochim. Acta*, 44 (1998) 633-642.
17. H. Zhang, J. Wang, Z. Wang, F. Zhang, S. Wang, *Synth. Met.*, 159 (2009) 277-281.
18. HL. Li, JX. Wang, QX. Chu, Z. Wang, FB. Zhang, SC. Wang, *J. Power Sources*, 190 (2009) 578-586.
19. JB. Zang, YH. Wang, XY. Zhao, GX Xin, SP Sun, XH. Qu, SB. Ren, *Int. J. Electrochem. Sci.*, 7 (2012) 1677-1687.
20. Y. Zhang, X. Jiang, R. Zhang, P. Sun, Y. Zhou, *Electrochim. Acta*, 56 (2011) 3264-3269.
21. R. Kiebooms, R. Menon, K. Lee, Synthesis, Electrical and Optical Properties of Conjugated Polymers, in: H.S. Nalwa (Ed.), Handbook of Advanced Electronic and Photonic Materials and Devices, Vol. 8. Conducting Polymers, Academic Press, New York, 2001, pp. 1-102.
22. Y. Harima, F. Ogawa, R. Patil, X. Jiang, *Electrochim. Acta*, 52 (2007) 3615-3620.
23. M. Žic, *J. Electroanal. Chem.*, 635 (2009) 29-38.
24. DH. Zhou, YH. Li, JY. Wang, P. Xu, XJ. Han, *Mater. Lett.*, 65 (2011) 3601-3604.
25. S. Quillard, G. Louarn, J. P. Buisson, M. Boyer, M. Lapkowski, A. Pron, S. Lefrant, *Synth. Met.*, 84 (1997) 805-806.
26. Y. Furukawa, F. Ueda, Y. Hyodo, I. Harada, T. Nakajima, T. Kawagoe, *Macromolecules*, 21 (1988) 1297-1305.
27. J. Tang, X. Jing, B. Wang, F. Wang, *Synth. Met.*, 24 (1988) 231-238.
28. G. Socrates, Infrared and Raman characteristic group frequencies. Table and charts, ed. John Wiley and Sons, Ltd, Chichester, 3rd edn, 2001, pp. 107–113, 123, 157–167, 176–177, 220–222.
29. L. Zhang, Y. Long, Z. Chen, M. Wan, *Adv. Funct. Mater.*, 14 (2004) 693-698.
30. J. Stejskal, I. Sapurina, M. Trchová, E. Konyushenko, P. Holler, *Polymer*, 47 (2006) 8253-8262.
31. I. Šeděnková, M. Trchová, J. Stejskal, *Polym. Degrad. Stab.*, 93 (2008) 2147-2157.

32. M. Trchová, E.N. Konyushenko, J. Stejskal, J. Kovářová, G. Ćirić-Marjanović, *Polym. Degrad. Stab.*, 94 (2009) 929-938
33. M. Trchová, J. Stejskal, *Pure Appl. Chem.*, 83 (2011) 1803–1817.
34. Z.D. Zujovic, L.J. Zhang, G.A. Bowmaker, P.A. Kilmartin, J. Travas-Sejdic, *Macromolecules*, 41 (2008) 3125-3135.
35. E. Dmitrieva, L. Dunsch, *J. Phys. Chem. B*, 115 (2011) 6401-6411.
36. G. Ćirić-Marjanović, N. Blinova, M. Trchová, J. Stejskal, *J. Phys. Chem. B*, 111 (2007) 2188-2199.
37. A. Kellenberger, E. Dmitrieva, L. Dunsch, *Phys. Chem. Chem. Phys.*, 13 (2011) 3411-3420.
38. A. Kellenberger, E. Dmitrieva, L. Dunsch, *J. Phys. Chem. B*, 116 (2012) 4377-4285.